



UNIVERSITY OF LEEDS

This is a repository copy of *Macro-Scale Tread Patterns for Traction in the Intestine*.

White Rose Research Online URL for this paper:

<http://eprints.whiterose.ac.uk/160007/>

Version: Accepted Version

---

**Article:**

Norton, JC [orcid.org/0000-0001-9981-5936](https://orcid.org/0000-0001-9981-5936), Boyle, JH [orcid.org/0000-0002-4219-9383](https://orcid.org/0000-0002-4219-9383), Alazmani, A [orcid.org/0000-0001-8983-173X](https://orcid.org/0000-0001-8983-173X) et al. (2 more authors) (2020) Macro-Scale Tread Patterns for Traction in the Intestine. IEEE Transactions on Biomedical Engineering, 67 (11). pp. 3262-3273. ISSN 0018-9294

<https://doi.org/10.1109/tbme.2020.2982242>

---

© 2020 IEEE. Personal use of this material is permitted. Permission from IEEE must be obtained for all other uses, in any current or future media, including reprinting/republishing this material for advertising or promotional purposes, creating new collective works, for resale or redistribution to servers or lists, or reuse of any copyrighted component of this work in other works.

**Reuse**

Items deposited in White Rose Research Online are protected by copyright, with all rights reserved unless indicated otherwise. They may be downloaded and/or printed for private study, or other acts as permitted by national copyright laws. The publisher or other rights holders may allow further reproduction and re-use of the full text version. This is indicated by the licence information on the White Rose Research Online record for the item.

**Takedown**

If you consider content in White Rose Research Online to be in breach of UK law, please notify us by emailing [eprints@whiterose.ac.uk](mailto:eprints@whiterose.ac.uk) including the URL of the record and the reason for the withdrawal request.



[eprints@whiterose.ac.uk](mailto:eprints@whiterose.ac.uk)  
<https://eprints.whiterose.ac.uk/>

# Macro-scale tread patterns for traction in the intestine

Joseph C. Norton\*, Jordan H. Boyle, Ali Alazmani, Pete R. Culmer and Anne Neville

**Abstract— Goal:** Tread patterns are widely used to increase traction on different substrates, with the tread scale, geometry and material being tailored to the application. This work explores the efficacy of using macro-scale tread patterns for a medical application involving a colon substrate – renowned for its low friction characteristics. **Methods:** Current literature was first summarized before an experimental approach was used, based on a custom test rig with *ex vivo* porcine colon, to assess different macro-scale tread patterns. Performance was based on maximising traction while avoiding significant trauma. Repeated testing (n=16) was used to obtain robust results. **Results:** A macro-scale tread pattern can increase the traction coefficient significantly, with a static traction coefficient of  $0.74 \pm 0.22$  and a dynamic traction coefficient of  $0.35 \pm 0.04$  compared to a smooth control ( $0.132 \pm 0.055$  and  $0.054 \pm 0.015$ , respectively. n=16). Decreasing the scale and spacing between the tread features reduced apparent trauma but also reduced the traction coefficient. **Conclusion:** Significant traction can be achieved on colon tissue using a macro-scale tread but a compromise between traction (large feature sizes) and trauma (small feature sizes) may have to be made. **Significance:** This work provides greater insight into the complex frictional mechanisms of the intestine and gives suggestions for developing functional tread surfaces for a wide range of clinical applications.

**Index Terms—** Biotribology, capsule robots, functional surfaces, intestinal friction, robotic endoscopy.

## I. INTRODUCTION

Colorectal cancer is one of the leading causes of cancer related death worldwide, with an estimated 1.8 million new cases estimated in 2018 [1, 2]. As with all cancers, early diagnosis, and hence an effective screening program, is key to patient survival [1]. Inflammatory bowel disease is another major gastrointestinal (GI) tract issue that is debilitating for the individual and requires careful clinical management [3]. Together, these contribute a significant burden on the healthcare system, with the cost estimate exceeding €18 billion per year in Europe alone [3, 4]. The current gold standard procedure to directly inspect the colon and assist with diagnosis

and management of these diseases is colonoscopy. However, despite its widespread use, it has a number of substantial shortcomings [5, 6] that have motivated the development of novel technologies such as capsule endoscopes and related robotic endoscopy devices. These may offer an effective solution and are currently being explored for minimally invasive access to the GI tract [7]. Many of these devices rely on contact-based propulsion, necessitating high traction against soft tissue without causing significant trauma; a requirement which also applies to surgical tools such as tissue graspers [8, 9]. Therefore, understanding and controlling the interaction between these innovative devices and the soft, sensitive tissues inside the human body is of great importance as it directly impacts their performance and the locomotion strategy of future concepts.

Achieving both high traction and low trauma is a major challenge because the intestine is a delicate and low friction substrate. Lyle *et al.* highlight the latter by reporting friction coefficients ranging from 0.0004 (between smooth steel and small intestine) to 0.018 (between a micro-patterned PDMS and small intestine) [10]. A smoother surface and thicker mucus layer mean it is arguably even harder to achieve a high friction coefficient on the colon. This challenge has motivated a number of groups to investigate different ways of augmenting friction and these typically fall into three categories: *Suction* – using a vacuum to adhere to the soft tissue [11]; *Muco-adhesives* – exploiting the adhesive interaction between a synthetic muco-adhesive and the biological mucus layer [12, 13]; and *Tread patterns* – increasing resistance by the physical interaction of a tread and the tissue substrate [14]. The suitability of each method depends greatly on the application. Considering the context of this work being mobile robots and surgical gaspers: Suction is typically used for static adhesion and is limited as it requires a complex, bulky mechanism to provide and control the vacuum [11]. Similarly, muco-adhesives can require time to make a chemical bond and tend to degrade over repeated reattachments [15-17]. Thus, using tread patterns is a comparatively simpler and more robust approach which is appropriate for this application of a sliding contact on tissue.

The aim of this work is to develop a functional tread pattern for the intestine – specifically the colon. In doing so, an additional goal is to summarise current state-of-the-art and gain further understanding of the friction mechanisms in this challenging environment. We summarise a broad range of literature and provide greater insight into optimising tread patterns for the colon, with potential translation to other

This work was supported by the 2011-2016 EU FP7 ERC project "CODIR: colonic disease investigation by robotic hydro colonoscopy", collaborative ERC between University of Dundee and the University of Leeds.

\*J.C. Norton is with the School of Electronic and Electrical Engineering, University of Leeds, Leeds, UK (email: j.c.norton@leeds.ac.uk). All other authors are with the School of Mechanical Engineering, University of Leeds, Leeds, UK.

applications and soft tissue substrates. First, current state-of-the-art in the design of tread patterns for the intestine and current theory on the associated mechanisms governing friction are reviewed (Section II). This is then used to direct the design (Section III) and experimental evaluation (Section IV) of a functional tread pattern for use on the colon. Emphasis is placed on functionality and so the tread is designed and tested to give repeatable traction in a worst-case scenario and on different regions of a pig colon. To better understand the macroscopic tread-tissue interaction, histological analysis of trauma and a wheel contact transitioning from static to high rotational speed are used – both currently lacking in literature. We show that a macro-scale tread pattern may be most appropriate in this context and give an indication of practical performance in terms of traction and trauma.

## II. TRACTION IN THE INTESTINE

In this work, tread patterns are broadly separated into two feature scales: *Micro-scale* and *Macro-scale*, where “micro” refers to tread patterns that have a largest feature size (width, height or space) no greater than 200  $\mu\text{m}$ , the approximate point from which features are visible without magnification and a threshold that separates the range of feature dimensions used in literature.

### A. State-of-the-art tread patterns for tissue substrates

Table 1 summarises current state-of-the-art micro- and macro-scale treads tested on tissue substrates. Both scale of tread patterns are shown to increase the friction coefficient on a tissue substrate, but with high variability and differing levels of success. The vast majority of studies use sliding, flat coupons for the experimental work and it is unclear how these treads perform in a more functional application of transitioning from stick (static) to slip (dynamic) and with loads and velocities applicable to mobile robots and surgical tools. Micro-scale tread patterns are shown to take inspiration from nature and attempt to mimic the micro-scale pillars found on the toe pads of tree frogs [18] and even some species of insect [19] and fish [20]. Traction and/or adhesion is increased through a number of mechanisms, including: increasing real contact (asperity-asperity contact [19, 21]) – i.e. encouraging boundary friction [22]; reducing crack propagation at the contact [22, 23] thus hindering stick-slip motion [19]; and encouraging the displacement and distribution of thin fluid layers on the surface of the substrate, further promoting boundary friction and increasing the effect of capillary forces [8, 19, 21-26]. Conversely, macro-scale treads depend primarily on the physical squeezing or deforming of tissue to increase traction and do not rely heavily on interaction with fluid layers.

Results on the trauma caused by these tread patterns are not given or are limited to qualitative observations. Outside of the context of tread patterns, Heijnsdijk *et al.* [9] investigated the trauma caused by a series of surfaces used for tissue grasping (e.g. during laparoscopic surgery), disregarding traction

performance. Pig colon tissue was clamped with 4-50 N normal load between two surfaces with various macro-scale patterns, including triangular ridges and hemispherical pillars. Only qualitative visual observations (e.g. tissue tear) were used in the results. Li *et al.* [27] investigated friction induced trauma to rabbit small intestine. A latex dome (contact area 105 – 118  $\text{mm}^2$ ) was pressed against the outside (serosa) of the small bowel with a normal force of 1 – 3 N. A sliding velocity of 10  $\text{mm/s}$  was used over 1 – 5 min of continuous sliding. A histological evaluation showed that a normal load of 1 N and sliding duration of 1 min caused little trauma and, while 2 N showed significantly more, the damage was still reversible. Despite the obvious limitations of the tissue being rabbit and the contact being made with the serosa and not the inside surface of the bowel (mucosa), this work gives an indication of acceptable loads and sliding durations for tread patterns.

### B. Frictional mechanisms in the intestine

The presence of a fluid and the properties of the substrate play a fundamental role in friction characteristics as they govern the interaction of the two surfaces. The colon, illustrated in Fig. 1 is thin-walled ( $1.08 \pm 0.24 \text{ mm}$  [28]), soft and viscoelastic ( $14 - 120 \text{ kPa}$ )<sup>1</sup> [29] and partially mobile within the abdomen. The shape of the lumen is defined by centimetre-scale ridges called haustra and the surface comprises millimetre-scale creases or ridges, 0.717 - 1.181 mm in height [30]. The mucosa is smooth and is made-up largely of crypt cells that give it a microscopic honeycomb-like appearance [31]. The tissue has multiple layers, the main being: Mucosa, submucosa, muscularis and serosa [28, 32, 33]. Specialised goblet cells continually secrete a viscous, non-Newtonian mucus over the mucosa. Compared to the rest of the GI tract, this mucus layer is thickest in the colon and has two distinct sub-layers: a loose outer layer and a base layer that is firmly adhered to the epithelium [34, 35]. The small intestine has similar mechanical properties [36] and tissue thickness [28, 37] but has a rougher surface texture due to the presence of villi [31, 38] and a thinner (both in terms of thickness and viscosity) mucus layer [34]. Both small intestine and colon have been investigated in literature and are used to inform this work as the minor differences do not detract from the major similarities: they are both soft and viscoelastic with a lubricious mucus layer.

The intestine is a complex biological substrate so the frictional characteristics cannot simply be described using the Coulombic friction theory. It is stated in [39], and demonstrated in literature (Table 1), that the total frictional resistance ( $F_t$ ) is velocity dependent and can be described by three distinct components, namely the Coulombic friction component ( $F_c$ ), Viscous friction component ( $F_v$ ) and Environmental friction component ( $F_e$ ) (1):

$$F_t(v) = F_c + F_v + F_e \quad (1)$$

<sup>1</sup> *In vivo* goat tissue under compression at different rates (0.02  $\text{mm/s}$  – 5  $\text{mm/s}$ ). Goat bowel tissue is a similar size to human.

Table 1 – Current state-of-the-art tread patterns. If not stated in the paper, the friction coefficient ( $\mu$ ) was calculated from the graphical results provided.

	Author	Experimental details	Results summary
Micro	Buselli <i>et al.</i> [40]*	Circular pillars. Diameter: 15 - 180 $\mu\text{m}$ ; Height: 100 $\mu\text{m}$ ; Spacing between pillars: 11.5 - 135 $\mu\text{m}$ . Linear velocity: 0.35 mm/s. Porcine colon.	$\mu$ of 0.17 - 0.4 (Control) to 0.23 - 0.75 (Treads)
	Zhang <i>et al.</i> [41]*	Circular pillars. Diameter: 60 - 140 $\mu\text{m}$ . Height: 100 $\mu\text{m}$ . Linear velocity: 0.25 mm/s. Rabbit small intestine.	$\mu$ between 0.19 (Control) and 0.12 - 0.34 (Treads)
	Glass <i>et al.</i> [42]*	Circular pillars. Diameter: 140 $\mu\text{m}$ . Height: 140 $\mu\text{m}$ . Spacing: 105 $\mu\text{m}$ . Linear velocity: 0.1 mm/s. Porcine small intestine.	$\mu$ of 0.09-0.25 (Control) to 0.15 - 0.4 (Tread).
	Lee <i>et al.</i> [14]*	Range of patterns including square pillars and straight grooves (both parallel and perpendicular orientated). Relative heights, widths and spaces between features approximately 65 $\mu\text{m}$ , 85 $\mu\text{m}$ and 65 $\mu\text{m}$ respectively. Linear velocity: 5 mm/s. Porcine colon.	$\mu > 1$ ‡
	Chen <i>et al.</i> [8]*	Polygon shaped pillars. Feature sizes approximately 140 $\mu\text{m}$ long, 50 $\mu\text{m}$ wide 30 $\mu\text{m}$ high and spaced 20 $\mu\text{m}$ apart. Linear velocity: 0.5 mm/s. Wetted liver.	$\mu$ of 0.45-0.9 Elongated hexagons performed best.
Macro	Accoto <i>et al.</i> [43]*	Rectangular grooves 2 mm wide and spaced 4 mm apart. Linear velocity: 5 mm/s - 14 mm/s. Porcine colon.	$\mu$ of 0.001 (Control) and 0.47-0.67 (Grooves).
	Wang <i>et al.</i> [44]*	Triangular, cylindrical and rectangular-shaped features; each feature approximately 1.5 mm wide. <i>No velocity stated.</i> Porcine colon.	$\mu$ of 0.3 - 0.69 (Control) and 0.85 - 0.88 (triangular ridges).
	Gao <i>et al.</i> [45]*	Array of circular holes, ring-shaped holes, parallel grooves, wavy parallel grooves, square-shaped holes and oblique or diamond-shaped holes. Depth of 0.5 mm and a width of 0.5 - 1 mm. <i>Carbopol polymer included as mucoadhesive. No velocity stated.</i> Porcine colon.	$\mu > 1$ † Diamond shapes performed best.
	Kim <i>et al.</i> [38]*	End-effectors with either rounded, flat or hollow-tipped tubes and with varying number of protrusions. Feature scale in the order of 1-10 mm. Linear velocity: 5 mm/s. Porcine small intestine.	$\mu > 1$ .
	Rentschler <i>et al.</i> [46]	Rotating cylinder with straight grooves, straight ridges, helical ridges and multiple brush-like bristles. Helical feature approximately 1.5 mm. Linear velocity: 10 mm/s. Bovine liver.	$\mu$ range of 0.12 - 0.17 (Helical tread).

\*Tread patterns placed on flat coupons.

†Assumed to be due to carbopol polymer used and the resulting muco-adhesion.

‡Patterns have a limited and highly variable impact due to dominant edge effects from coupon.

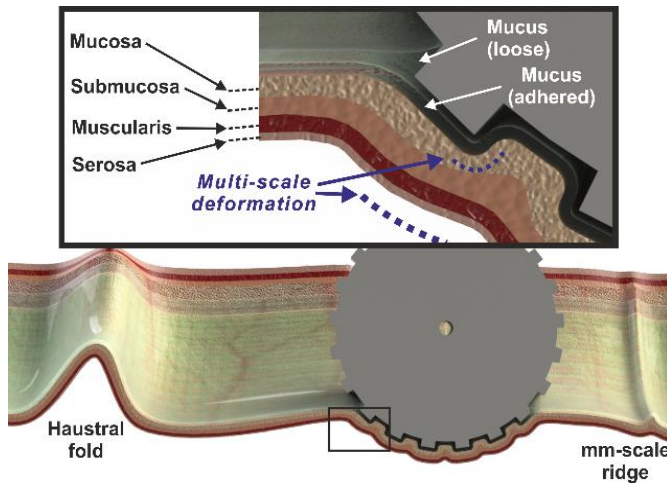


Fig. 1. Wheel-intestine interaction. An illustration of a macro-scale tread pattern interaction with colon tissue, showing both the anatomy and scales of deformation.

*Coulomb friction* ( $F_c$ ) is the product of the normal force between the two substrates ( $N$ ) and the Coulombic friction coefficient ( $\mu_c$ ) (2):

$$F_c = \mu_c N \quad (2)$$

This component is dependent on the degree of asperity-asperity contact which is maximised by matching the surface roughness of the two substrates [30]. Therefore, it necessitates direct contact with the tissue epithelium and, in the context of the intestine, a microscopic roughness.

*Viscous friction* ( $F_v$ ) is the resistance resulting from the apparent viscosity ( $\delta$ ) of the intestinal mucus and the relative velocity of the two substrates ( $v$ ) (3):

$$F_v = \delta v \quad (3)$$

The intestinal mucus is a shear-thinning fluid so the apparent viscosity decreases with increasing shear rate [47]. While static, the tacky mucus provides an adhesive force and then, during shear, resistance comes from the viscosity of the mucus which opposes shear force [47-49].

*Environmental resistance* ( $F_e$ ) is sometimes referred to as “edge-effects” [10] or losses due to tissue hysteresis [43]. It is shown to be the dominant form of resistance on intestinal tissue [38] and is described as the force required to deform or displace the tissue around the object (or tread feature). It is proportional to the strain dependent pressure resulting from the elastic restoring force of the tissue acting on the tread feature ( $P(x)$ ), the amount of tissue “gripped” by the treads ( $S$ ) and the angle

of the applied force relative to the object-tissue contact patch ( $\theta$ ) (4):

$$F_e = P(x)S\sin(\theta) \quad (4)$$

When the angle is  $90^\circ$  (substrate normal to tread face),  $F_e$  is maximised as the resistance directly opposes motion. When the angle is  $0^\circ$  or  $180^\circ$  (substrate and tread feature parallel),  $F_e$  is zero as no tissue is displaced/deformed during motion. This interaction of the tread with the tissue is also discussed in [44]. Due to the viscoelastic properties of the tissue, velocity will have a significant effect on this resistance as  $P(x)$  is dependent on the modulus of the tissue and high shear rates result in a higher modulus [29, 39, 48, 49].

### III. FUNCTIONAL TREAD DESIGN

Achieving functional traction is essential to the efficient locomotion of mobile robots and to the effective, safe use of surgical graspers. We define a “functional” tread pattern as:

- Producing a minimum net tractive effort in the order of 1 N [50, 51]. For example, this equates to a traction coefficient of 0.34 for the robot described in [52].
- Effective at speeds in excess of 5 mm/s to ensure their efficacy when interacting with tissue, e.g. the mobile robot in [52].
- Providing repeatable traction on all regions of the colon, in both static and dynamic (slip) conditions, without readily clogging with debris.
- Rapidly and completely displacing fluid (e.g. water and mucus) from the substrate to ensure high traction and controllability.
- Not causing trauma beyond the mucosal layer as the underlying submucosa contains vessels [14, 40].

The principles summarised in Section II, combined with knowledge of the anatomy, frictional characteristics and results from experimental work in literature, were used to guide the design (tread feature scale, geometry and material) and evaluation of a functional tread pattern capable of high traction and low trauma on the colon.

#### A. Tread feature scale

Here we consider the applicability of each feature scale as the starting point for the design of a functional tread pattern. Micro-scale tread patterns are designed to closely match the roughness of the intestine and so could theoretically maximise asperity-asperity contact [40, 48]. Additionally, the treads are too small to penetrate to the more critical underlying tissue layers (submucosa) [14, 53] and so are inherently safe. However, several limitations reduce their effectiveness in this context:

The micro-scale treads must completely displace (“de-wetting” [54]) mucus layers that can be thicker than the height of the tread features. Naturally, microscopic treads become easily flooded [26], particularly in the colon where the firmly adhered mucus layer alone can be in excess of  $150 \mu\text{m}$  thick [34]. There is a high probability of a layer of mucus remaining between the tread and the tissue epithelium - particularly under

low loads. Resistance is likely to come almost entirely from the mucus (i.e.  $F_v$ ) [26, 41]. Micro-scale pillars can reduce hydrodynamic repulsion and encourage the displacement of liquid from a contact [24, 26] but their effectiveness at rapidly displacing thick, viscous fluid layers is limited [19]. Therefore, while static and at very low velocities, resistance between such treads and intestinal tissue is expected to be primarily from the adhesive bond between the mucus and the tread features. This may explain the high friction coefficient at low normal loads for the micro-scale treads in Table 1, as the coefficient is calculated by dividing the resistance ( $F_t$ ) by the normal load and mucus properties are not dependent on load (as indicated by [53] and [30]). The lack of direct contact means that the maximum traction - and indeed tractive effort - will be limited by the rheological properties of the mucus [49] and controlling traction using normal load would be largely ineffective; This is highlighted by the fact that the friction coefficients of the micro-scale patterns mentioned in Table 1 were seen to reduce by 43 - 80% [14, 40, 42] with an increase in normal load. This effect may be worsened by mucus being progressively squeezed out of the tissue, enhancing lubrication [43, 48] and likely further preventing real contact with the tissue substrate. Another limitation of these treads is that the intestinal tissue provides very little resistance to deformation and so on the micro-scale, it is probable that even if the mucus was completely displaced and direct asperity-asperity contact was made, resistance from the resulting deformation of these microscopic asperities (i.e.  $F_e$ ) will be extremely low. Lastly, when considering the practical use of micro-treads, it is logical that the features can become easily clogged with small debris preventing them from effectively interacting with the substrate. This could include tissue debris remaining attached to the treads [14] and an organic layer (e.g. dehydrated mucus) adhered to their surface [41]. The individual pillars/treads are also susceptible to damage and their fabrication is complex [30, 55]. In summary, micro-scale tread patterns should be considered most appropriate for low sliding speeds, low normal loads and use on clean substrates with a very thin (or no) mucus layer – for example, on surgical graspers used for manipulating liver tissue [56].

Based on the environment, current literature, the functional requirements and limitations of micro-scale tread features, we propose that a macro-scale tread pattern is most appropriate for use on the intestine. To exploit  $F_e$ , high stress concentrations are favoured as they allow more tissue to be ‘squeezed’ between the tread features to provide resistance [38, 47]. This mechanism is less dependent on asperity-asperity interaction and mucus properties, and more on the volume of tissue displaced by the tread features [33]. These treads suit applications with higher sliding speeds and normal loads; Literature supports this with coefficients which, although generally lower than those achieved with micro-scale treads, reducing by only 3 - 30 % [43, 44] with increasing normal load. This is particularly important for surgical tools as it allows effective control, where increasing load increases traction. An additional, practical benefit of increasing the scale of the treads is an increase in mechanical robustness and manufacturability.

### B. Tread geometry

Any macro-scale tread pattern will deform soft tissue and provide some resistance to shear. However, tread geometry has a clear influence on traction by impacting both the hydrodynamics and tissue interaction.

*Hydrodynamics* - Effective de-wetting of the surface reduces hydrodynamic lubrication and increases the degree and speed of tread-substrate contact. A high groove volume (space between tread features) and grooves perpendicular to the shear direction are most effective at de-wetting a tyre-road contact [57]. Furthermore, a hierarchy of grooves significantly reduces hydrodynamic repulsion, resulting in faster and more complete de-wetting of the contact under reduced normal load [24, 26]. Torrent frogs combine these features and use a hierarchical array of pillars on their toes [19, 55, 58, 59]; here, the dense array of channels allows liquid to flow out, reducing hydrodynamic repulsion to facilitate de-wetting [22, 24]. The resulting more intimate contact increases friction through contact with the environment. Elongating the pillars has been shown to increase performance on a synthetic wetted surface, although the exact mechanism is unclear [8, 25, 58].

*Tissue interaction* - Once fluid is displaced from the contact, tissue must deform into the tread grooves before  $F_e$  can be exploited. There are two design features governing this: (1) groove volume to surface area ratio, which affects stress concentrations and the volume of tissue resisting deformation, and (2) the orientation and shape of the features which must encourage tissue ingress while also having a high density of perpendicular edges to provide resistance [25, 33]. In literature, perpendicular edges give the highest level of resistance because tissue cannot easily slide around them, as it would with circular pillars [33, 45]. Parallel grooves provide the least obstruction to the tissue during shear, but being aligned with the direction of shear ensures that the soft tissue readily enters into the tread. It has been proposed that diamond-shaped grooves [45], or similar shaped elongated hexagons, will provide superior traction to other simple tread shapes. They are shown to promote de-wetting while also increasing  $F_e$ . The shape encourages the ingress of tissue *and* provides an edge to resist the elastic restoring force meaning they should perform well during shear.

### C. Tread material

There is a paucity of literature available on how the mechanical properties of treads effect traction in the intestine. It is likely that a compromise has to be made, as a hard material is beneficial to deform the tissue (increasing  $F_e$  and reducing tread degradation from wear), while a soft material is advantageous in improving tread-tissue contact by conforming to the surface [25]. A soft material could also reduce trauma by preventing highly localised stress concentrations [33]. To simplify fabrication and better understand the friction mechanisms a rigid plastic will be used here, with material properties explored in future work

### D. Design summary

It is hypothesised that a rigid, macro-scale tread pattern with elongated, perpendicularly orientated polygon features (in this case: elongated hexagons) can provide superior, functional traction at a rotating contact compared to other simple feature geometries and a control (smooth on the macro scale).

A macro-scale is most appropriate for a tread pattern (for use on the intestine under functional loads and velocities) primarily because of the low modulus of the tissue and the thick, adhered mucus layer. Polygons, such as hexagons, can be tightly and efficiently packed together to create a large surface area, high density of gripping edges, as well as a large channel volume [19]. The large surface area distributes force and so reduces trauma [8]. The interlocking channels are effective at rapidly de-wetting a surface and promoting tissue interaction [58]. The multifaceted shape of the pillars with a high edge density may also provide high  $F_e$  on soft substrates, as shown by the use of a similar pattern in [45]. Using elongated hexagons has been shown to improve friction results [8, 58] but the best orientation is unclear and so both should be explored.

## IV. EXPERIMENTAL METHOD

To test the hypothesis, a number of core geometries were included in an experimental study: A control (smooth on the macro scale), parallel grooves (Pa), perpendicular grooves (Pe), elongated hexagons with parallel orientation (H.Pa) and elongated hexagons with perpendicular orientation (H.Pe). The work was carried-out in three stages. *Stage 1* was used to validate which of the 5 distinct tread geometries (including the control) resulted in the highest traction. In *Stage 2*, the aspect ratio and scale of the best performing tread geometry were modified to optimise the balance of traction and trauma. In *Stage 3*, the individual tread patterns were placed under load and continuous slip and the resulting tissue trauma was observed.

A tread feature height of 500  $\mu\text{m}$ , width of 750  $\mu\text{m}$  (elongated hexagons length: 1500  $\mu\text{m}$ ) and aspect ratio (tread feature width:space) of 1:1 were chosen on the basis of preliminary experimental work and macro-scales reviewed in literature [33, 44]. H.Pe performed best in preliminary work so several variants were produced in an attempt to optimise it further: H.Pe.0.5 (1:0.5 aspect ratio), H.Pe.0.5.s (1:0.5 aspect ratio and smaller features) and H.Pe.s (1:1 aspect ratio and smaller features). For the smaller H.Pe variants, the height and width of the treads were reduced by 33% to 330 and 500 $\mu\text{m}$  respectively. Fig. 2 shows all of these tread patterns. The wheels were approximately 7mm in width and 16mm in diameter, based on the dimensions of the robot in [52]. They were manufactured out of a rigid plastic resin (HTM140, EnvisionTEC, flexural modulus of 3350 MPa and an elongation at break of 3.5%) using a 3D printer (EnvisionTEC, Perfactory 3 mini) chosen for its precision. The microscale surface roughness ( $R_z$ ), consisting of perpendicular grooves which are a by-product of the 3D printing technique, was measured as 6.4  $\mu\text{m}$  using a contactless profilometer device (*Alicona Infinite Focus*) and is a comparable scale to the features in the colon.

### A. Test environment

The test conditions aimed to balance *in-vivo* conditions (synonymous with complexity) with repeatability. The critical variables were controlled as accurately as possible using a custom made test rig (Fig. 3). The main features of the setup are:

- *Controllable Normal force application* (between wheel and substrate) - The wheel was pressed into the substrate with a known, controllable force.
- *Rotating wheel/contact* - A torque was applied to the wheel via a DC motor and the tractive effort measured using a precision load cell.
- *Biological substrate* - A pig colon substrate with a compliant backing and an intact, hydrated mucus layer was used.

Referring to Fig. 3: A clamp (a.) was used to hold the colon tissue sample on top of a block of soft silicone (b.) (Shore 00-30), used to loosely represent the tissue in the abdomen<sup>2</sup>. This assembly was placed on a low friction linear ball-bearing slide (c.) and was connected to a precision Bed load cell (*Transducer Technique*, GS0-150) (d.) via a rigid steel rod. This setup allowed any shear force applied to the tissue to be precisely measured by the load cell with minimal losses. To assess the functional performance of the tread patterns, the drivetrain from the robot prototype [52] (e.) was used to rotate the wheel. A stiff, lightweight bracket (f.) secured this assembly to a separate linear ball-bearing slide perpendicular to the substrate (g.). This allowed the wheel assembly to be lowered onto the surface and isolated any torque applied by the motor from the Beam load cell. The Beam load cell (h.) was secured to a third linear ball-bearing slide (i.). The Beam load cell rests on a pivot point above the wheel bracket. The combined mass was applied as a normal, passive load (weight) to the tissue. An adjustable spring (j.) counteracted this and was used to set the desired normal load. A motor controller (*ESCON 24/2*) was used to control the desired motor current (torque) and a real-time DAQ (cRIO, National Instruments) was used to acquire all the data. Example data from the Bed load cell is shown in (k.). A typical traction profile from a single repetition consists of two distinct features: a sharp increase to a peak traction value (*Static traction*) followed by a return to a lower value (*Dynamic traction*) where the wheel is in a slip regime. The results were summarised by two traction coefficients that were used to describe the overall performance of the tread: The *Static traction coefficient* ( $\mu_s$ ) was calculated by dividing the peak (static) traction by the corresponding normal load at that instant; the *Dynamic traction coefficient* ( $\mu_d$ ) was calculated by dividing the average traction over a steady-state five seconds of the run (chosen from the median time while in continuous slip) by the mean normal load over the same five seconds. Although normal load was not altered during tests, a mean was used to account for variations due to dynamic wheel-tissue interactions.

Fresh porcine colons were acquired from an abattoir on the day of testing. The pigs were all 5 – 6 months old and the distal 1 m of the colon was used. The tissue was gently rinsed with water to remove any residual faecal matter before being placed in a container of phosphate buffered saline solution to prevent dehydration and degradation. All tests were completed within 5 hours (below the 10 hours suggested by Kim *et al.* [38]) and at room temperature. As the purpose of this work was to determine the functional performance of tread patterns, worst-case environmental conditions were used where possible. These included:

- *A strained substrate* – This was done to control the overall shape of the substrate and ensure some repeatability in terms of macro-scale substrate features. Lyle *et al.* suggest that placing the tissue under stress may be a more “natural representation of the tissue mechanics *in vivo*” [10]. The stress (induced by stretching the specimen with 193g) was calculated to be similar to the hoop stresses seen during colonoscopy insufflation.
- *A flooded substrate* – Liquid may be present in the colon (e.g. if water is used to distend or clean the lumen) so we flooded the substrate with saline solution. This keeps the mucus layer hydrated (low viscosity) and evaluates the treads’ ability to displace liquid from the contact during slip.

### B. Traction test protocol

Each wheel was washed in isopropyl alcohol to remove any residue before being attached to the motor assembly for testing. It was then lowered onto the tissue sample and the desired normal load applied. To evaluate the 750  $\mu\text{m}$  scale treads, loads of 245 mN and 490 mN were used. These were chosen based on the available force from a mobile robotic device ([50, 60]) and are within safe limits stated in [27]. Within 20 s of the wheel contacting the tissue, demand current to the DC motor was increased linearly from zero over 20 s during which the wheel transitioned from static to dynamic traction. The estimated speed of the motor during continuous slip was 90 rpm (corresponding to ca. 81 mm/s linear shear rate). A new area of the tissue specimen was used for the next repetition. This was done for a total of four repetitions per specimen, with four tissue specimens being used for each tread (two from the distal end of the colon segment and two from the proximal end), resulting in a total of 16 repetitions per tread geometry/load combination.

### C. Trauma test protocol

Similar conditions to the traction tests were used, but in this case the wheel was placed rapidly into continuous slip for 10 s using a step current input. Higher normal loads of 490 mN, 980 mN and 1960 mN were used as no trauma was observed during the 245 mN tests. A single repetition was carried out per load and tread type.

<sup>2</sup> The *in vivo* mechanical properties of general abdominal tissue is difficult to determine and is not present in literature. A soft silicone was used to provide some repeatable and reusable compliance.

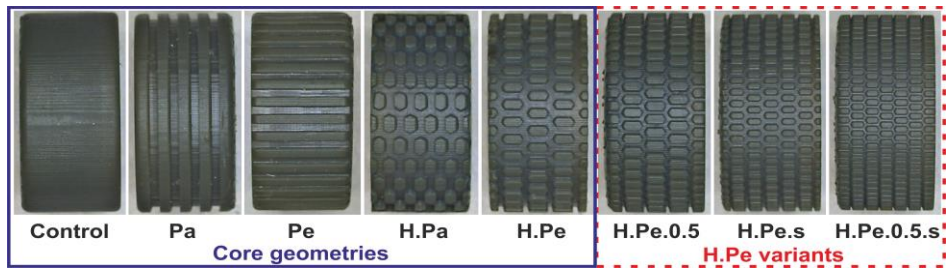


Fig. 2 – The 3D printed tread patterns used.

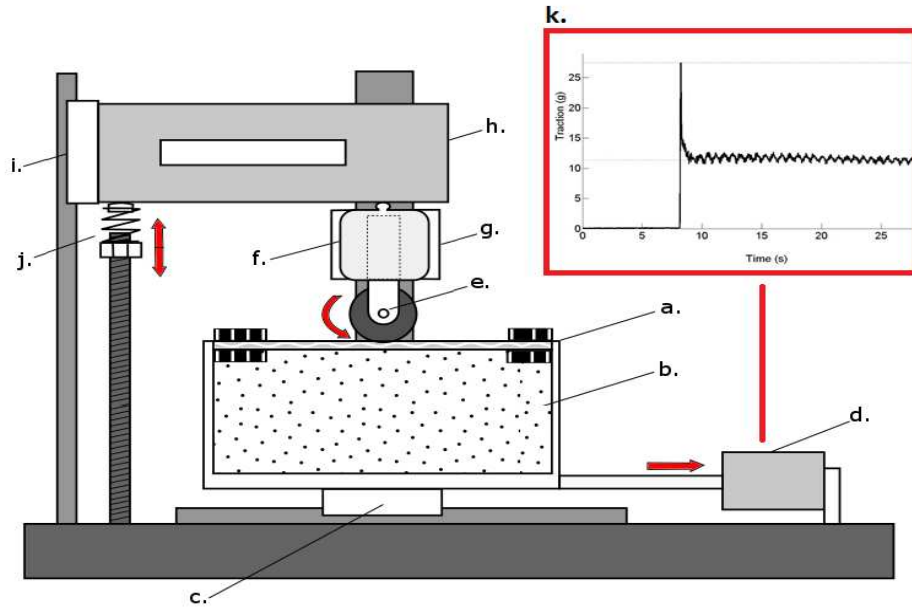


Fig. 3 – A schematic of the test rig, showing all key components: a. Colon tissue held in a clamp, b. soft silicone backing, c. horizontal linear ball bearing slide, d. precision load cell, e. wheel (with tread) assembly, f. wheel bracket, g. vertical linear ball bearing slide, h. beam load cell, i. second vertical linear ball bearing slide, j. spring counterbalance and k. example force output.

The contact patches from each repetition were stained with black India ink, excised before being placed in individual test tubes, fixed using a 10% formalin solution and then stored in Ethanol. The samples were then sent for histological analysis. Three slices were taken across each sample to increase the probability of acquiring a representative cross-sectional view of the trauma caused. Each slice was inspected for abnormal, mechanically induced trauma. The most severe was selected as the representative sample and ranked using Table 2. Focus was placed solely on mucosal trauma (damage due to the mechanical wear caused by friction) and whether it extends beyond this layer. This was for a number of reasons: (1) The normal loads and contact time were within safe limits suggested in literature [27], so reducing the chance of pressure related trauma, (2) The treads only contact the mucosa and (3) Trauma confined to the mucosa is deemed acceptable as it does not contain any critical vasculature.

Table 2 - The scale used to determine degree of trauma. Example histology slices annotated with features.

	Description	Example slice
0	No features visible (mucosa intact, no abnormalities detected)	* Mucosa
1	Small features (very small cuts in upper portion of mucosa)	
2	Medium features (noticeable cuts into or thinning of the mucosa)	
3	Large features (cuts through, or complete erosion of mucosa)	

\*Example interaction of wheel (parallel tread) with mucosa

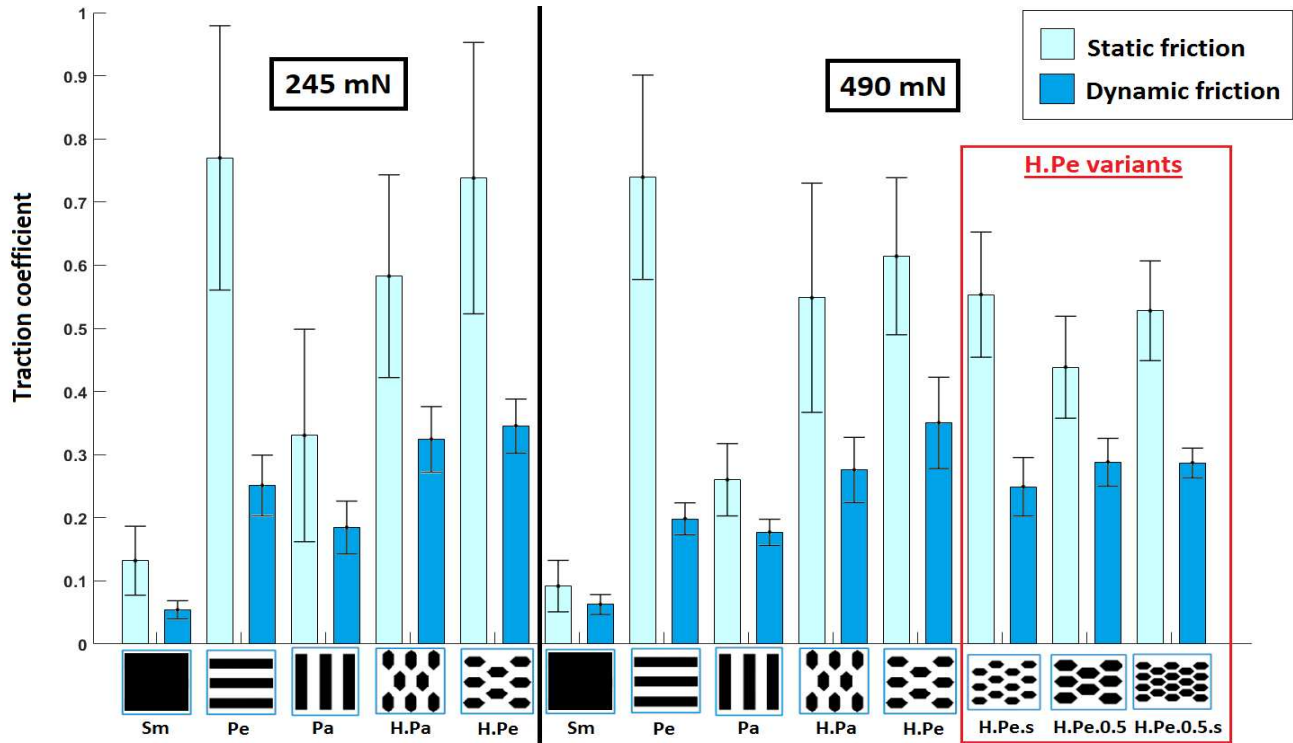


Fig. 4 - Bar chart of traction results. Showing both the static ( $\mu_s$ ) and dynamic traction coefficients ( $\mu_d$ ) of all the tread patterns under 245 mN and 490 mN normal loads. n = 16. Whiskers show the standard deviation of the mean value.

Table 3 – Trauma results. Maximum degree of trauma seen after 10 s continuous slip for each tread, and the suggested safe load. (Tread patterns placed in order of increasing trauma).

Tread:	Sm	Pa	H.Pe.0.5.s	H.Pe.s	Perp	H.Pe.0.5	H.Pe	H.Pa
Trauma:	0-1	0-1	1-2	1-2	2-3	3	3	3
Max Load (mN):	1960	1960	1960	1960	980	490	490	490

### V. RESULTS

Results were successfully obtained for all planned test cases. The variation in results across different colon samples was inspected by applying the T-test to results from different colons and regions. It was seen that the majority of the results showed no statistically significant difference ( $p > 0.05$ ) between traction coefficients from the same tread on different colon specimens (54% of the dynamic cases and 77% of the static cases). Lyle *et al.* [10] found similar, non-statistically significant results. This, in addition to the requirement of having a functional tread pattern for use on all regions of the colon, suggested that the results from each tread pattern could be combined across all colons and colon samples to facilitate direct comparison of performance between the various treads. The traction coefficients ( $\mu_s$  and  $\mu_d$ ) of all treads are shown in Fig. 4 and the trauma results are summarised in Table 3.

As expected,  $\mu_s > \mu_d$  and the results showed a high level of variance which is particularly evident in the static case. Under static conditions the control had a mean coefficient of  $0.112 \pm 0.068$  and the highest  $\mu_s$  was achieved by the Pe tread ( $0.755 \pm 0.264$ ), closely followed by the H.Pe tread ( $0.676 \pm 0.248$ ). During slip, H.Pe had the highest  $\mu_d$  of  $0.348 \pm 0.084$ , closely followed by H.Pa which had a  $\mu_d$  of  $0.300 \pm 0.0731$  (compared to  $0.058 \pm 0.021$  for the Control).

Reducing the aspect ratio of H.Pe to 1:0.5 reduced  $\mu_s$  by 28.6% ( $p < 0.05$ ) and  $\mu_d$  by 17.7% ( $p < 0.05$ ). With a 1:1 aspect ratio, reducing the scale reduced  $\mu_s$  by 10% ( $p > 0.05$ ) and  $\mu_d$  by 28.9% ( $p < 0.05$ ). However, with the 1:0.5 aspect ratio, reducing the scale did not have a clear impact, giving a 20% ( $p < 0.05$ ) increase in  $\mu_s$  and no significant change in  $\mu_d$ . Of these reduced scale treads, H.Pe.s had the highest  $\mu_s$  of  $0.553 \pm 0.099$  and H.Pe.0.5.s had the highest  $\mu_d$  of  $0.287 \pm 0.023$ .

In most cases the traction coefficient decreased slightly as normal load increased, but with limited statistical significance: For  $\mu_s$ , the control showed the greatest reduction of 30.5% ( $p < 0.05$ ) while Pa, H.Pe, H.Pa and Pe showed reductions of 21.2% ( $p > 0.05$ ), 16.8% ( $p > 0.05$ ), 6.0% ( $p > 0.05$ ) and 4.0% ( $p > 0.05$ ) respectively. In the dynamic case, the control and H.Pe showed an increase in  $\mu_d$  of 16.1% ( $p > 0.05$ ) and 1.4% ( $p > 0.05$ ) respectively, while Pe, Pa and H.Pa all showed a reduction in  $\mu_d$  of 21.1% ( $p < 0.05$ ), 4.3% ( $p > 0.05$ ) and 14.8% ( $p < 0.05$ ).

Table 3 ranks the tread patterns in order of increasing trauma. The control, Pa, H.Pe.s and H.Pe.0.5.s all caused acceptable levels of trauma (i.e. confined to the mucosa), even up to loads of 1960 mN. The Perp tread showed acceptable levels of trauma up to 980 mN of normal load, but clearly eroded the mucosa at 1960 mN. H.Pe, H.Pa and H.Pe.0.5 all showed significant levels of trauma above loads of 490 mN.

## VI. DISCUSSION

### A. Tread geometry and feature scale

The tread geometry was shown to greatly affect the traction coefficient. A perpendicular orientation in the tread patterns had a clear advantage, as  $\mu_s$  and  $\mu_d$  for Pe and H.Pe were greater than their parallel counterparts (Pa and H.Pa)<sup>3</sup>. Interestingly, the performance of the Pe tread - which had the highest  $\mu_s$  - greatly decreased when slip was introduced. This supports the hypothesis that perpendicular orientated features provide greatest resistance while static, but parallel channels are needed to encourage tissue ingress during shear. Hexagonal features thus provide a beneficial combination of the two. The control had a higher traction coefficient than similar controls in literature, which was attributed to the micro-scale build features that result from 3D printing fabrication (in this case, lines perpendicular to the direction of shear). This also supports the hypothesis that that micro-scale ridges/grooves (and perhaps micro-scale treads in general) perform badly in the colon under more functional loads and shear rates.

The scale and aspect ratio of the H.Pe tread were altered. Reducing either the aspect ratio or scale resulted in a decrease in both  $\mu_s$  and  $\mu_d$ . This supports the theory that environmental resistance (tread groove volume and high stress concentrations) dominates over tread contact area [33, 38, 61]. A balance between high stress concentrations (high traction) and high contact area (low trauma) must be made.

### B. Traction and load dependence

It was shown in literature that the friction coefficient against intestinal tissue decreases with increasing load. The exact mechanism is unclear, but it is suggested that increasing the load squeezes out mucus and water from the mucosa [43, 48], reducing tissue contact (environmental resistance) and limiting the traction coefficient to the rheological properties of the mucus. The results in this study somewhat support this, showing a max reduction of 21.2% - similar to that seen in literature [43, 44]. This understanding is important as it both impacts traction control (how traction changes with changing load input) and shows that a macro-scale tread may have the least variability with load.

### C. Trauma

Trauma confined to the upper region of the mucosa was considered acceptable as this does not contain vasculature [14]. Considering the thickness and low modulus of the tissue, trauma was less than expected. This may be because the dual mucus layer creates a “slippage” plane [62] and effectively protects the underlying tissue during shear. The larger features of H.Pe and H.Pa caused significant trauma at low loads, presumably due to the high stress concentrations created at each tread feature. Reducing the feature scale and aspect ratio both affect trauma by altering these stress concentrations and more effectively distributing the load.

### D. Experimental limitations

Assessing the trauma caused by each tread pattern was challenging, as the tissue substrate is highly variable from specimen to specimen. It is also difficult to complete an accurate assessment of the trauma across the entire contact patch by only visualising very thin (4  $\mu\text{m}$ ) slices from three separate sites. The storing and handling of the samples may have resulted in the tissue layers delaminating; however, focusing on the mucosa negated this potential issue. Slicing the sample in the correct region also proved difficult but the use of 3 slices spaced apart increased confidence.

The temperature of the tissue was kept at room temperature from dissection to experimental evaluation and the tissue properties are altered by this reduced temperature and the lack of blood supply [38, 49]. Saline solution was used to flood the substrate which would have altered the properties of the mucus, with the viscosity expected to be lower compared to *in vivo* due to dilution [62, 63]. However, traction from macro-scale treads is less dependent on mucus properties so this was not considered problematic. Because of the experimental complexities it is difficult to say whether our results over or underestimate the friction coefficients. For example, *in-situ* tests were shown to give lower friction coefficients (presumably due to higher temperature, muscle tone, mucus replenishment and maintained blood flow to the area) by Lyle *et al.* [49]. Despite these uncertainties, the number of repetitions used in this study are higher than those previously reported, and combined with the repeatable method and worst-case conditions used, give the results greater robustness and confidence with regard to the expected performance macro-scale tread patterns in real applications.

### E. Future recommendations

The effect that velocity and tread material properties (mechanical and chemical) have on traction and trauma were not studied in this work. These should be investigated in more detail as literature shows conflicting results, or none at all. Optimising tread stiffness could increase the traction coefficient and reduce trauma. A more biologically accurate substrate (as used by Lyle [10]) could also be used in future.

There was a clearly visible difference in variance between the static and dynamic cases. Variance was lower under dynamic conditions, suggesting that the traction mechanism is more consistent during continuous slip. One theory for this high variance and difference between static and dynamic cases relates to the start conditions of the tests: The time in contact with the tissue and its macroscopic features are likely to introduce variability in the degree of tread-tissue interlocking (volume of tissue deformed) and the thickness of the mucus layer at the interface. After a period of continuous slip, the mucus is likely to have been displaced and the tissue features

<sup>3</sup> When comparing H.Pe and H.Pa, the results for the 245 mN load were different, but not statistically significant.

flattened producing a more consistent interface and so less overall variance between repetitions.

## VII. CONCLUSION

We have shown that a macro-scale tread pattern greatly increases the traction coefficient against colonic tissue compared to a control (smooth wheel with micro-scale features). This suggests that contact-based propulsion of mobile robots could be a feasible concept for gastrointestinal exploration. Tread geometry has a significant effect on the traction coefficient, with tread patterns consisting of hexagonal pillars and straight grooves, both arranged orthogonally to the direction of shear, giving the highest static traction coefficient. During slip, hexagonal pillars (both parallel and perpendicular orientations) had the highest dynamic traction coefficient. Reducing the scale and the spacing between the pillars generally reduced the traction coefficient, indicating that traction is primarily from environmental resistance. The large scale hexagonal tread patterns caused significant trauma, while the other geometries and the smaller scale hexagonal patterns caused acceptable levels. From the treads tested, the reduced scale (330 $\mu$ m height and 500 $\mu$ m width) hexagonal pillars with a perpendicular orientation provides the best balance of traction and trauma.

## ACKNOWLEDGMENT

This work is funded by the 2011-2016 EU FP7 ERC project "CODIR: colonic disease investigation by robotic hydro colonoscopy", collaborative ERC between University of Dundee (PI Prof Sir A Cuschieri) and the University of Leeds (PI Prof Anne Neville). The authors would like to thank the CoDIR team, particularly the lead investigators Sir Alfred Cuschieri and Prof. Anne Neville, for their support on this work. The research is also supported by the National Institute for Health Research (NIHR) infrastructure at Leeds. The views expressed are those of the authors and not necessarily those of the NHS, the NIHR or the Department of Health.

## REFERENCES

1. Siegel, R.L., et al., *Colorectal cancer statistics, 2017*. CA Cancer J Clin, 2017. **67**(3): p. 177-193.
2. Bray, F., et al., *Global cancer statistics 2018: GLOBOCAN estimates of incidence and mortality worldwide for 36 cancers in 185 countries*. Ca-a Cancer Journal for Clinicians, 2018. **68**(6): p. 394-424.
3. Kaplan, G.G., *The global burden of IBD: from 2015 to 2025*. Nat Rev Gastroenterol Hepatol, 2015. **12**(12): p. 720-7.
4. Luengo-Fernandez, R., et al., *Economic burden of cancer across the European Union: a population-based cost analysis*. Lancet Oncology, 2013. **14**(12): p. 1165-1174.
5. Hafner, M., *Conventional colonoscopy: technique, indications, limits*. Eur J Radiol, 2007. **61**(3): p. 409-14.
6. Seeff, L.C., et al., *How many endoscopies are performed for colorectal cancer screening? Results from CDC's survey of endoscopic capacity*. Gastroenterology, 2004. **127**(6): p. 1670-1677.
7. Toennies, J.L., et al., *Swallowable medical devices for diagnosis and surgery: The state of the art*. Proceedings of the Institution of Mechanical Engineers, Part C: Journal of Mechanical Engineering Science, 2016. **224**(7): p. 1397-1414.
8. Chen, H., et al., *Bioinspired Surface for Surgical Graspers Based on the Strong Wet Friction of Tree Frog Toe Pads*. ACS Appl Mater Interfaces, 2015. **7**(25): p. 13987-95.
9. Heijnsdijk, E.A., et al., *Slip and damage properties of jaws of laparoscopic graspers*. Surg Endosc, 2004. **18**(6): p. 974-9.
10. Lyle, A.B., J.T. Luftig, and M.E. Rentschler, *A tribological investigation of the small bowel lumen surface*. Tribology International, 2013. **62**: p. 171-176.
11. Ge, D., et al., *Quantitative study on the attachment and detachment of a passive suction cup*. Vacuum, 2015. **116**: p. 13-20.
12. Dodou, D., P. Breedveld, and P.A. Wieringa, *Mucoadhesives in the gastrointestinal tract: revisiting the literature for novel applications*. Eur J Pharm Biopharm, 2005. **60**(1): p. 1-16.
13. Smart, J.D., *The basics and underlying mechanisms of mucoadhesion*. Adv Drug Deliv Rev, 2005. **57**(11): p. 1556-68.
14. Lee, S.H., et al., *An Optimal Micropatterned End-Effector for Enhancing Frictional Force on Large Intestinal Surface*. ACS Applied Materials & Interfaces, 2010. **2**(5): p. 1308-1316.
15. Dodou, D., P. Breedveld, and P.A. Wieringa, *Friction manipulation for intestinal locomotion*. Minim Invasive Ther Allied Technol, 2005. **14**(3): p. 188-97.
16. Dodou, D., P. Breedveld, and P.A. Wieringa, *Stick, unstick, restick sticky films in the colon*. Minim Invasive Ther Allied Technol, 2006. **15**(5): p. 286-95.
17. Dodou, D., et al., *Mucoadhesive films inside the colonic tube: performance in a three-dimensional world*. J R Soc Interface, 2008. **5**(28): p. 1353-62.
18. Drotlef, D.M., et al., *Morphological studies of the toe pads of the rock frog, *Staurois parvus* (family: Ranidae) and their relevance to the development of new biomimetically inspired reversible adhesives*. Interface Focus, 2015. **5**(1).
19. Varenberg, M. and S.N. Gorb, *Hexagonal Surface Micropattern for Dry and Wet Friction*. Advanced Materials, 2009. **21**(4): p. 483-+.
20. Wainwright, D.K., et al., *Stick tight: suction adhesion on irregular surfaces in the northern clingfish*. Biol Lett, 2013. **9**(3): p. 20130234.
21. Barnes, W.J.P., *Functional Morphology and Design Constraints of Smooth Adhesive Pads*. MRS Bulletin, 2011. **32**(6): p. 479-485.
22. Federle, W., et al., *Wet but not slippery: Boundary friction in tree frog adhesive toe pads*. J R Soc Interface, 2006. **3**(10): p. 689-97.
23. Drotlef, D.M., et al., *Insights into the Adhesive Mechanisms of Tree Frogs using Artificial Mimics*. Advanced Functional Materials, 2013. **23**(9): p. 1137-1146.
24. Gupta, R. and J. Frechette, *Measurement and Scaling of Hydrodynamic Interactions in the Presence of Draining Channels*. Langmuir, 2012. **28**(41): p. 14703-14712.
25. Iturri, J., et al., *Torrent Frog-Inspired Adhesives: Attachment to Flooded Surfaces*. Advanced Functional Materials, 2015. **25**(10): p. 1499-1505.
26. Persson, B.N.J., *Wet adhesion with application to tree frog adhesive toe pads and tires*. Journal of Physics-Condensed Matter, 2007. **19**(37).
27. Li, W., et al., *Investigation on Friction Trauma of Small Intestine In Vivo Under Reciprocal Sliding Conditions*. Tribology Letters, 2014. **55**(2): p. 261-270.
28. Marchesini, R., et al., *Ex-Vivo Optical-Properties of Human Colon Tissue*. Lasers in Surgery and Medicine, 1994. **15**(4): p. 351-357.
29. Higa, M., et al., *Passive mechanical properties of large intestine under in vivo and in vitro compression*. Medical Engineering & Physics, 2007. **29**(8): p. 840-844.
30. Buselli, E., et al., *Evaluation of friction enhancement through soft polymer micro-patterns in active capsule endoscopy*. Measurement Science and Technology, 2010. **21**(10): p. 105802.
31. Shamsuddin, A.M., P.C. Phelps, and B.F. Trump, *Human Large Intestinal Epithelium - Light-Microscopy, Histochemistry, and Ultrastructure*. Human Pathology, 1982. **13**(9): p. 790-803.
32. Ellis, H., *Anatomy of the caecum, appendix and colon*. Surgery (Oxford), 2011. **29**(1): p. 1-4.
33. Gao, P., et al., *Microgroove cushion of robotic endoscope for active locomotion in the gastrointestinal tract*. International Journal of Medical Robotics and Computer Assisted Surgery, 2012. **8**(4): p. 398-406.
34. Atuma, C., et al., *The adherent gastrointestinal mucus gel layer: thickness and physical state in vivo*. American Journal of Physiology-Gastrointestinal and Liver Physiology, 2001. **280**(5): p. G922-G929.
35. Johansson, M.E., J.M. Larsson, and G.C. Hansson, *The two mucus layers of colon are organized by the MUC2 mucin, whereas the*

- outer layer is a legislator of host-microbial interactions. *Proc Natl Acad Sci U S A*, 2011. **108 Suppl 1**: p. 4659-65.
36. Egorov, V.I., et al., *Mechanical properties of the human gastrointestinal tract*. *Journal of Biomechanics*, 2002. **35**(10): p. 1417-1425.
  37. Finkelstone, L., E. Wolf, and M.W. Stein, *Etiology of small bowel thickening on computed tomography*. *Canadian Journal of Gastroenterology*, 2012. **26**(12): p. 897-901.
  38. Kim, Y.T. and D.E. Kim, *Biotribological investigation of a multi-tube foot for traction generation in a medical microrobot*. *Proceedings of the Institution of Mechanical Engineers Part H- Journal of Engineering in Medicine*, 2009. **223**(H6): p. 677-686.
  39. Zhang, C., et al., *Modeling of Velocity-dependent Frictional Resistance of a Capsule Robot Inside an Intestine*. *Tribology Letters*, 2012. **47**(2): p. 295-301.
  40. Buselli, E., et al., *Evaluation of friction enhancement through soft polymer micro-patterns in active capsule endoscopy*. *Measurement Science and Technology*, 2010. **21**(10).
  41. Zhang, H.Y., et al., *Friction Enhancement between Microscopically Patterned Polydimethylsiloxane and Rabbit Small Intestinal Tract Based on Different Lubrication Mechanisms*. *ACS Biomaterials Science & Engineering*, 2016. **2**(6): p. 900-907.
  42. Glass, P., E. Cheung, and M. Sitti, *A Legged Anchoring Mechanism for Capsule Endoscopes Using Micropatterned Adhesives*. *Ieee Transactions on Biomedical Engineering*, 2008. **55**(12): p. 2759-2767.
  43. Accoto, D., et al. *Measurements of the frictional properties of the gastrointestinal tract*. in *World Tribology Congress*. 2001.
  44. Wang, K.D. and G.Z. Yan, *Research on measurement and modeling of the gastro intestine's frictional characteristics*. *Measurement Science and Technology*, 2009. **20**(1).
  45. Gao, P., et al., *Microgroove cushion of robotic endoscope for active locomotion in the gastrointestinal tract*. *Int J Med Robot*, 2012. **8**(4): p. 398-406.
  46. Rentschler, M.E., S.M. Farritor, and K.D. Lagnemma, *Mechanical design of robotic in vivo wheeled mobility*. *Journal of Mechanical Design*, 2007. **129**(10): p. 1037-1045.
  47. Lai, S.K., et al., *Micro- and macrorheology of mucus*. *Advanced Drug Delivery Reviews*, 2009. **61**(2): p. 86-100.
  48. Kim, J.S., et al., *Experimental investigation of frictional and viscoelastic properties of intestine for microendoscope application*. *Tribology Letters*, 2006. **22**(2): p. 143-149.
  49. Lyle, A.B., et al., *Preliminary Friction Force Measurements on Small Bowel Lumen When Eliminating Sled Edge Effects*. *Tribology Letters*, 2013. **51**(3): p. 377-383.
  50. Valdastrì, P., et al., *A New Mechanism for Mesoscale Legged Locomotion in Compliant Tubular Environments*. *Ieee Transactions on Robotics*, 2009. **25**(5): p. 1047-1057.
  51. Quirini, M., et al., *Design and fabrication of a motor legged capsule for the active exploration of the gastrointestinal tract*. *Ieee-Asme Transactions on Mechatronics*, 2008. **13**(2): p. 169-179.
  52. Norton, J., et al., *RollerBall: a mobile robot for intraluminal locomotion*. 2016 6th Ieee International Conference on Biomedical Robotics and Biomechatronics (Biorob), 2016: p. 254-259.
  53. Lee, S.H., et al., *An optimal micropatterned end-effector for enhancing frictional force on large intestinal surface*. *ACS Appl Mater Interfaces*, 2010. **2**(5): p. 1308-16.
  54. Persson, B.N.J., *Wet adhesion with application to tree frog adhesive toe pads and tires*. *Journal of Physics: Condensed Matter*, 2007. **19**(37): p. 376110.
  55. Drotlef, D.-M., et al., *Insights into the Adhesive Mechanisms of Tree Frogs using Artificial Mimics*. *Advanced Functional Materials*, 2013. **23**(9): p. 1137-1146.
  56. Chen, H.W., et al., *Bioinspired Surface for Surgical Graspers Based on the Strong Wet Friction of Tree Frog Toe Pads*. *ACS Applied Materials & Interfaces*, 2015. **7**(25): p. 13987-13995.
  57. Fwa, T., et al., *Effectiveness of Tire-Tread Patterns in Reducing the Risk of Hydroplaning*. *Transportation Research Record: Journal of the Transportation Research Board*, 2009. **2094**: p. 91-102.
  58. Iturri, J., et al., *Torrent Frog-Inspired Adhesives: Attachment to Flooded Surfaces*. *Advanced Functional Materials*, 2015. **25**(10): p. 1499-1505.
  59. Murarash, B., Y. Itovich, and M. Varenberg, *Tuning elastomer friction by hexagonal surface patterning*. *Soft Matter*, 2011. **7**(12): p. 5553-5557.
  60. Norton, J., et al. *RollerBall: A mobile robot for intraluminal locomotion*. in *2016 6th IEEE International Conference on Biomedical Robotics and Biomechatronics (BioRob)*. 2016.
  61. Zhang, C., et al., *Modeling of Velocity-dependent Frictional Resistance of a Capsule Robot Inside an Intestine*. *Tribology Letters*, 2012. **47**(2): p. 295-301.
  62. Cone, R.A., *Barrier properties of mucus*. *Adv Drug Deliv Rev*, 2009. **61**(2): p. 75-85.
  63. Yoshida, H., Y. Morita, and K. Ikeuchi, *Biological lubrication of hydrated surface layer in small intestine*. *Tribol. Interface Eng. Ser.: Tribol. Res. Des. Eng. Syst*, 2003. **41**: p. 425-428.